

# Formation of hydrogen atoms in the 2s and 2p states by neutralization of H<sup>-</sup> ions in gases

V. I. Radchenko and G. D. Ved'manov

Ural State Technical University, 620002 Ekaterinburg, Russia

(Submitted 30 November 1994)

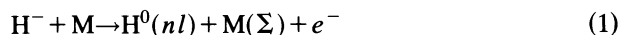
Zh. Éksp. Teor. Fiz. **107**, 1204–1220 (April 1995)

A technique is presented, together with results of an experimental determination of the cross sections  $\sigma_{i_0}(2s;2p)$ , for forming hydrogen atoms  $H(2s_{1/2};2p_{1/2,3/2})$  by neutralizing H<sup>-</sup> ions with energies  $E = 1.15, 5.0, 6.9, \text{ and } 10.4$  MeV in gaseous He, Ar, Kr, Xe, H<sub>2</sub>, O<sub>2</sub>, and CO<sub>2</sub> targets. The cross sections were measured by recording the  $L_\alpha$  radiation of H atoms with the help of a photomultiplier which operated in the single-photon regime and was placed directly in the collision chamber. Formulas have been obtained for calculating the desired cross sections from the experimental data. It is found that the  $\sigma_{i_0}(2s;2p)$  cross sections for the various gaseous targets, as functions of the energy of the H<sup>-</sup> ions, behave in a way similar to the dependences  $\sigma_{01}(E)$  and  $\sigma_{i_0}(E)$  so that their ratio remains approximately constant over the investigated energy range and equal to  $\sigma_{i_0}(2s)/\sigma_{i_0}(2p) \approx 2-2.7$ . The influence of various experimental factors on the results and the measurement error is analyzed. © 1995 American Institute of Physics.

## 1. INTRODUCTION

A study of the processes of neutralization of fast H<sup>-</sup> ions in various media and the scattering of H<sup>+</sup>, H<sup>0</sup>, and H<sup>-</sup> particles without change of their charge would provide a powerful basis both for the development of ground breaking theoretical concepts of the physics of ion-atom interactions and for the solution of a number of important applied problems (such as, for example, energy transport by a particle beam over significant distances, the heating and diagnostics of plasmas in setups with controllable thermonuclear synthesis, etc.). Among the entirety of such processes, a central place must be given to the problem of forming hydrogen atoms in various excited states. Actually, excited hydrogen atoms have substantially larger electron-detachment collision cross sections and significantly shorter lifetimes with respect to electron detachment in an efficiently acting electric field.<sup>1-3</sup> In addition to this, cascade transitions in the de-excitation of atoms make an atomic beam "visible" over a wide range of electromagnetic frequencies, which makes it possible, in particular, to realize contact-free control of the intensity and spatial-angular characteristics of the beam, etc.

Quite a large number of experimental studies have been carried out on collisions which form hydrogen atoms in excited states, among which we may mention only a few<sup>4-7</sup> associated with the use of H<sup>-</sup> ion beams and the determination of the  $\sigma_{i_0}(nl)$  cross sections by recording the photon flux arising as a result of the decay of the  $nl$ -states of the hydrogen atom. Like these efforts, the overwhelming majority of studies on primary H<sup>+</sup> and H<sup>0</sup> particle beams have also examined the particle energy range  $E < 100$  keV for inert-gas as well as N<sub>2</sub> and O<sub>2</sub> targets. Measurement data on cross sections of processes of the type



are absent in the region of higher collision energies; here the symbol  $\Sigma$  means that the final state of the target particle M

can belong either to the discrete spectrum or the continuum. This is a consequence of the fact that the desired cross sections  $\sigma_{i_0}(nl)$  fall off at higher energies accompanied by a correspondingly abrupt growth in the complexity of experimental setups intended to provide absolute measurements of the photon flux, taking Doppler broadening, relativistic shift, and polarization into account, and, in a number of cases, also "quantum beats" of the radiation intensity which arise due to interference of close-lying excited states of the hydrogen atom in the electric field.

Theoretical calculations of total and doubly differential cross sections of processes of type (1) can be found in Refs. 8–12, based on a very approximate description of colliding systems before and after the interaction. These calculations have been carried out only in a selective way in the region  $E \leq 1.5$  MeV for atomic hydrogen, inert gases, and  $n = 1$  and 2. Detailed, systematic calculations of the differential and total electron-detachment cross sections of collisions of the type (1) over a wide range of energies of the H<sup>-</sup> ions, for various targets and values of the quantum numbers  $n, l$ , are lacking. One of the main obstacles to the realization of such calculations consists in the problem of choosing the wave function of the free state of the electron lost by the H<sup>-</sup> ion.

In this paper, which is a continuation of a series (Refs. 13–15), we outline a technique and present results of measurements of absolute values of cross sections of formation of hydrogen atoms in the  $2s_{1/2}$  and  $2p_{1/2,3/2}$  states by neutralization of H<sup>-</sup> ions with energies  $E = 1.15, 5.0, 6.9, \text{ and } 10.4$  MeV in rarefied gaseous He, Ar, Kr, Xe, H<sub>2</sub>, O<sub>2</sub>, and CO<sub>2</sub> targets.

## 2. EXPERIMENTAL SETUP. MEASUREMENT TECHNIQUE

The technique we used to measure the  $\sigma_{i_0}(2s;2p)$  cross sections is based on recording the H-atom  $L_\alpha$  radiation generated in the course of the collisions (1) directly in the collision chamber and is in many ways similar to the technique

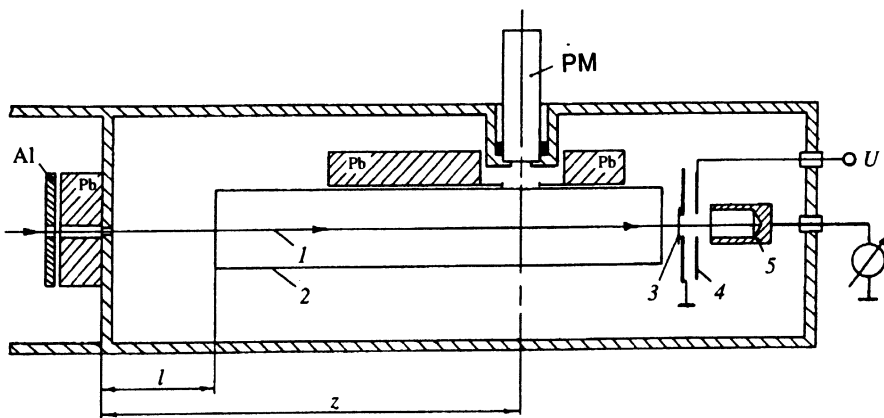


FIG. 1. Diagram of experimental setup for recording  $L_\alpha$  radiation of fast hydrogen atoms: 1—particle beam, 2—quenching capacitor, 3—aluminum foil, 4—guard electrode, 5—Faraday cylinder.

used in Refs. 7 and 16. The  $\sigma_{i0}(2s)$  cross sections are determined by increasing the intensity of the  $L_\alpha$  radiation by applying a constant electric field to the “beam-gas” interaction region, which leads to an abrupt shortening of the lifetimes of the hydrogen atoms in the metastable  $2s_{1/2}$  state. The main distinguishing feature of our technique consists in using a single-photon channel to record the Lyman- $\alpha$  radiation. The reason for doing this is that for the  $H^-$  ion current levels ( $\sim 10^{-11}$  A) reached in our experiment while optimizing the other parameters the  $L_\alpha$ -photon flux impinging on the sensor area of the detector is roughly 100/photons/s.

The  $H^-$  ions are accelerated in a classical U-120 cyclotron and after passing through the beam transport channel enter the collision chamber through the entrance opening, which has a diameter of 1.5 mm. That part of the experimental setup intended for recording the  $L_\alpha$  radiation and measuring the  $H^-$  current is depicted schematically in Fig. 1. The gas pressure in the collision chamber was determined with the help of an individually calibrated manometric converter (with a measurement error of 5–7%) and was varied over the range  $2.7 \cdot 10^{-3}$ – $1.3$  Pa depending on the sort of gas, the cross section of the process ( $\bar{\sigma}$ ) for  $H^-$  ions of given energy and other factors. Traversing a distance  $l = 130$  mm from the entrance collimator, the beam then passes between the plates of a capacitor in order to quench the metastable  $2s$  state of the hydrogen atoms and then after passing through a sheet of aluminum foil and a guard electrode it enters a Faraday cylinder.

The radiation generated by the interaction of the beam particles with the target gas is detected with the help of a photomultiplier (a prototype unit, analogous to an FÉU-142) with a combination box-louvre dipole system and CsI photocathode. The photomultiplier is set up perpendicular to the beam axis and the electric field vector  $F$  of the quenching capacitor at a distance  $z = 400$  mm from the entrance opening of the collision chamber. The photomultiplier is inserted into a compressed gas cylinder of stainless steel; the vacuum seal is effected by a rubber washer around the housing of the photomultiplier in such a way that the entrance window of the photomultiplier is located in the vacuum space of the collision chamber, and the base, in the atmosphere. The voltage divider and the accelerator-electric pulse generator are located in the immediate vicinity of the base of the photomultiplier. The accelerator-pulse generator works as an inte-

grating amplitude discriminator, assigning the threshold level for cutoff of noise signals; the output pulses of the generator are recorded by a programmed counter. Together with another counter which receives signals from a “current-frequency” converter, which measures the charge brought in by the ions into the Faraday cylinder, the single-photon recording channel forms a synchronously controllable system, the number of induced photons recorded in which corresponds to a given number of ions arriving in the collision chamber.

Figure 2 shows the relative spectral sensitivity  $S_a$  for the given photomultiplier unit. The shortwave limit  $\lambda \approx 110$  nm of the sensitivity region of the photomultiplier is determined by the transparency zone of the  $MgF_2$  crystal serving as the entrance window of the photomultiplier. Since the amplitude distribution of the pulses arriving at the photomultiplier under the action of monoenergetic radiation from its sensitivity region is exponential in character, the value of the threshold level of the discriminator is chosen as low as possible above the level of the internal noise of the optical channel, but so as to provide the highest possible signal-to-noise ratio. In sum, the working parameters of the optical channel were maintained at values for which the frequency of arrival of the noise pulses did not exceed 0.1 pulse/s and the signal-to-noise ratio was not worse than 10–15. For the same param-

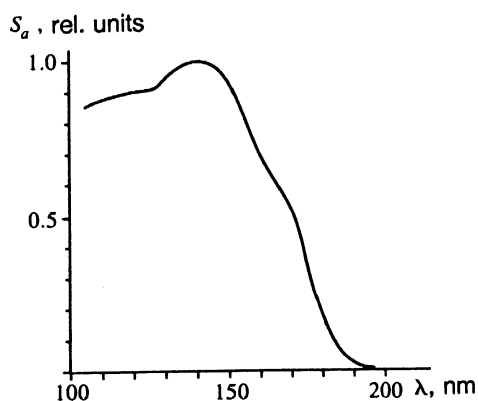


FIG. 2. Relative spectral sensitivity of the photomultiplier.

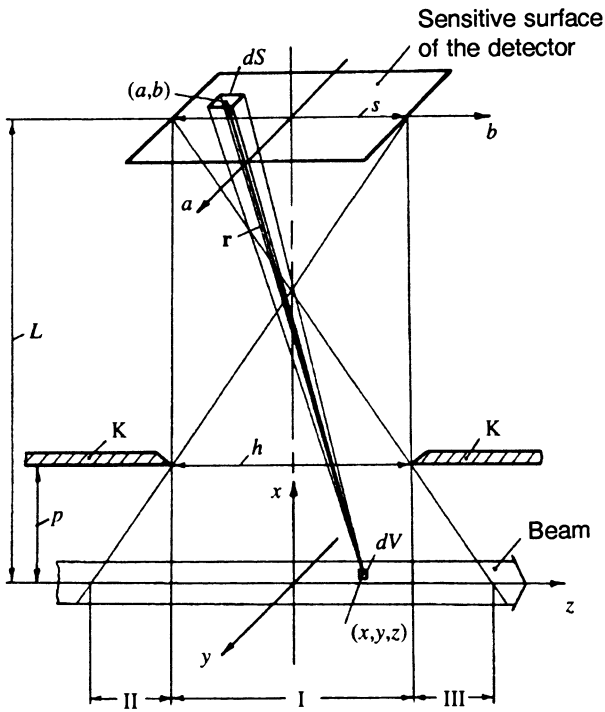


FIG. 3. Geometrical diagram of the setup for recording  $L_\alpha$  radiation.

eters the quantum efficiency of recording in the optical channel of the  $L_\alpha$  line stood at  $\eta=6.65\%$ .

Preliminary measurements, performed without passing the primary  $H^-$  ion beam into the collision chamber (the beam was held back entirely by a diaphragm placed over the entrance window), revealed the presence of background signals from the photomultiplier produced by the interaction of the penetrating secondary radiation with the structural elements of the photomultiplier and the setup. The intensity of the background signals grows rapidly with increase of the energy, and for  $E=10.4$  MeV is comparable to the intensity of the useful events. To eliminate these background signals, protective lead blocks were placed in the region of the entrance collimator and around the entrance window of the photomultiplier (see Fig. 1). This measure allowed us to almost completely eliminate these background signals.

Now let us find the ratio between  $N_r$ , the number of photons recorded by the photomultiplier per unit time, and the linear flux density  $dN_{h\nu}/dz$  of the generated radiation. Let  $\rho(x, y, z)$  be the volume density of the radiation at the point  $(x, y, z)$ , and  $\varepsilon(x, y, z; a, b)$  be the efficiency of recording of the radiation at the point  $(x, y, z)$  by the surface element  $dS$  of the sensitive zone of the detector at the point  $(a, b)$  on its surface (see Fig. 3). The vector joining the indicated points is denoted as  $\mathbf{r}$ . Then, the photon flux recorded by the surface element  $dS$  of the detector coming from the elementary volume  $dV=dxdydz$  is equal to

$$dN_r = \varepsilon \cdot \rho \cdot A(\theta, \varphi) \cdot dV \cdot \frac{d\Omega}{4\pi} = \varepsilon \cdot I(\theta, \varphi) \cdot d\Omega, \quad (2)$$

where  $d\Omega$  is the solid angle within which the surface element  $dS$  of the detector is "seen" from the point  $(x, y, z)$ ;

$A(\theta, \varphi) = I(\theta, \varphi) / \bar{I}$  is the coefficient of anisotropy of the radiation, which is defined in terms of the intensity  $I(\theta, \varphi)$  of the radiation flux per unit solid angle in the direction  $\mathbf{r}$ , defined by the polar angle  $\theta$  and azimuthal angle  $\varphi$ ;

$$\bar{I} = \frac{1}{4\pi} \int I(\theta, \varphi) d\Omega = \frac{I_0}{4\pi} \quad (3)$$

is the average radiation intensity;  $I_0 = \rho dV$  is the total radiation intensity (flux, in units of photons/second). Note that Eq. (3) gives us the normalization condition for the anisotropy

$$\frac{1}{4\pi} \int A(\theta, \varphi) d\Omega = 1. \quad (4)$$

Generally speaking, radiation produced by the interaction of the particle beam with the target or by the de-excitation of an atomic system in the presence of an external field is polarized and has an anisotropic angular distribution. The direction of motion of the particles or the electric field vector define the physical axis with respect to which the angle  $\theta$  is reckoned. It can be assumed<sup>17</sup> that the emerging dipole radiation is generated by three electric dipoles, one of which lies along the physical axis; the other two have the same moment (in magnitude) and are perpendicular to each other and the first dipole. Utilizing the fact that the intensity of the dipole radiation in directions making an angle  $\chi$  with the dipole axis is proportional to  $\sin^2\chi$ , it is easy to obtain the expressions

$$I(\theta) = \frac{3I_0[1 - P(\pi/2)\cos^2\theta]}{4\pi[3 - P(\pi/2)]}, \quad (5)$$

$$P(\theta) = \frac{P(\pi/2)\sin^2\theta}{1 - P(\pi/2)\cos^2\theta}, \quad (6)$$

where  $P(\theta) = (I_{\parallel} - I_{\perp}) / (I_{\parallel} + I_{\perp})$  is the polarization coefficient of the radiation observed at the angle  $\theta$  to the physical axis. Here  $I_{\parallel}(\theta)$  is the intensity of the radiation radiated at the angle  $\theta$  with electric field vector lying in the plane defined by the radiation wave vector and the physical axis, and  $I_{\perp}(\theta)$  is the intensity of the radiation with electric field vector perpendicular to the indicated plane. Since the momenta of the two last dipoles are equal, none of the quantities entering into expressions (5) and (6) depend on the azimuthal angle  $\varphi$ . For the "magic" angles  $\theta_m = 54.7^\circ$  and  $125.3^\circ$  the dependence of the intensity (5) on the degree of polarization vanishes, so that  $I(\theta_m) = I_0/4\pi = \bar{I}$  as in the absence of polarization, when  $P=0$ .

For the analysis that is to follow we introduce characteristic dimensions of the sensor zone in our set-up (see Fig. 3). The sensitive region (photocathode) of the photomultiplier is located a distance  $L=38.5$  mm from the beam axis and has an effective diameter of 7.0 mm. The clipping slit K is rectangular in shape, with length  $h=41.0$  mm along the beam and width 10 mm, and is located a distance  $p=15.0$  mm from the beam axis. The relatively small transverse dimensions of the beam and photocathode in comparison with the distance  $L$ , together with the fact that the efficiency  $\varepsilon$  of the given photomultiplier when recording the photons arriving from region I of the beam (Fig. 3) does not depend on the angle of incidence of the radiation or the coordinates  $(a, b)$

of the photocathode, allow a significant simplification in the calculations which are to follow. It should also be borne in mind that the efficiency of recording monoenergetic radiation can vary depending on the spectral characteristic of the detector (Fig. 2) as a consequence of variations in the wavelength  $\lambda$  of the radiation due to the Doppler and relativistic effects<sup>18</sup>:

$$\lambda = \lambda_0 \frac{1 - \beta \cos \varphi}{\sqrt{1 - \beta^2}}, \quad (7)$$

where  $\varphi$  is the angle between the direction of motion of the photon and the velocity vector  $\mathbf{v}$  of the particle that emitted it;  $\lambda_0$  is the wavelength of the photon emitted by the atom at rest;  $\beta = v/c$ ; and  $c$  is the speed of light. Thus, the wavelength  $\lambda_0 = 121.6$  nm of the  $L_\alpha$  radiation from the interaction region I (Fig. 3) even for  $H^-$  ions with maximal energy  $E = 10.4$  MeV varies only within the limits of 111.5 nm to 134.1 nm, which gives us the right to set  $\varepsilon(x, y, z; a, b) \equiv \eta(\lambda_0) = \text{const}$ .

Taking into consideration all of the above, we can write

$$d\Omega = \frac{S \sin^3 \alpha}{L^2}, \quad dz = \frac{L d\alpha}{\sin^2 \alpha},$$

where  $S$  is the area of the photocathode,  $\alpha$  is the angle between the beam axis  $\mathbf{z}$  and the look direction  $\mathbf{r}$ , and  $\rho dx dy = dN_{\hbar\nu}/dz$  is the linear photon flux density for the entire cross section of the beam. In the absence of an electric field  $\alpha = 0$ , and in the presence of an electric field  $\alpha$  and  $\theta$ , generally speaking, do not coincide. Substituting these differentials and also expression (5) into formula (2), it is easy to show that under the given experimental conditions, both in the presence of an external field and without, allowing for the polarization of the radiation can lead to variations in the recorded photon flux of less than 20%, which is roughly two times less than the statistical error of the measurements. On this basis, and also for the reason that we did not measure the polarization coefficient of the radiation in the present work, we will take the angular distribution of the  $L_\alpha$  radiation to be isotropic, i.e., we will set  $P = 0$  and  $A(\theta) = 1$ . In addition, the total contribution of the radiating regions II and III for the chosen experimental geometry to the total number  $N_r$  of recorded signals does not exceed 5% and can be completely ignored. Finally, the quantity  $dN_{\hbar\nu}(z)/dz$  depends weakly (practically linearly) on  $z$  in region I and can be taken to be constant in the integral (2) over  $dz$  (or, what is the same thing, over  $d\theta$ ), so we set it equal to the linear radiation density at the intersection point of the beam and photomultiplier axes:

$$N_r = \frac{\eta S z_1}{2\pi L \sqrt{z_1^2 + L^2}} \frac{dN_{\hbar\nu}(z)}{dz}, \quad (8)$$

where

$$2z_1 = h + \frac{h-s}{L-p} p$$

is the length of the radiating region I (Fig. 3). Under the conditions of our experiment

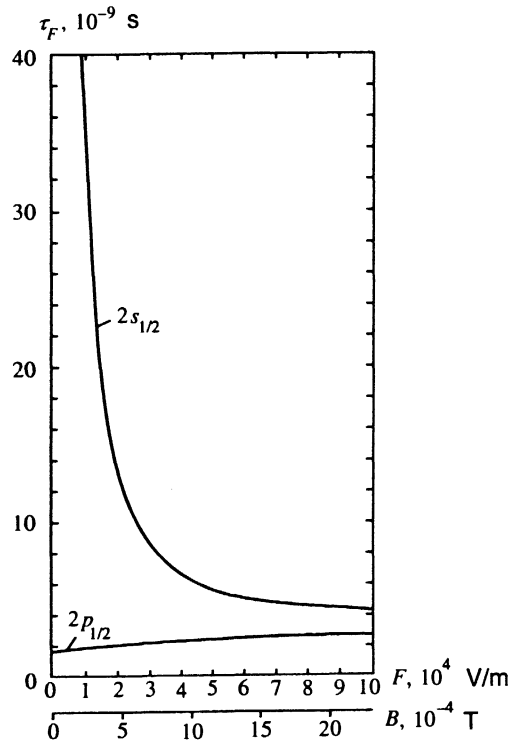


FIG. 4. Lifetime of hydrogen atoms in the  $2s_{1/2}$  and  $2p_{1/2}$  states in an electric field  $F$ . The second horizontal axis gives the magnetic induction field  $B$  that induces an electric field  $F = vB$  for hydrogen atoms moving perpendicular to it with energy  $E = 10$  MeV.

$$N_r = 6.68 \cdot 10^{-4} \frac{dN_{\hbar\nu}}{dz}.$$

The assumptions made in the derivation of relation (8) are such that changes resulting from them in the exact relation between  $N_r$  and  $dN_{\hbar\nu}/dz$  tend to cancel each other out and do not add up to any noticeable systematic error.

The electric field, which breaks the metastable  $2s_{1/2}$ -state of H atoms, was created by the current given to the capacitor plates.

The capacitor plates were positioned symmetrically about the beam axis (Fig. 1) and consisted of copper sheets 0.5 mm in thickness, 30 mm wide, and 520 mm long, polished and rigidly mounted in place 9.6 mm apart.

In the absence of an external field the metastable state of the hydrogen atom has a lifetime  $\tau(2s) = 0.1215$  s (Ref. 19) and decays with the emission of two correlated photons. In a weak electric field  $F < 1$  kV/cm Stark mixing of the  $2s_{1/2}$  and  $2p_{1/2}$  states takes place, which leads to an abrupt decrease in the lifetime  $\tau_F(2s)$  of the metastable atoms and some increase in the lifetime of the  $2p$  state,  $\tau_F(2p)$ . In the literature it is customary to denote the state of the hydrogen atom in an electric field by the same quantum numbers as in the absence of a field. We will follow that practice here. The rigorous quantum-mechanical theory of the calculation of the lifetimes of hydrogen atoms with  $n = 2$  in weak electric fields was constructed by Bethe and Salpeter.<sup>20,21</sup> Results of calculations carried out within the framework of this theory are shown in Fig. 4.

We determined the  $\sigma_{i0}(2s)$  cross section for two values of the electric field strength: for the ion energy  $E=1.15$  MeV,  $F=150$  V/cm (the corresponding lifetimes are  $\tau_F(2s)=20.5$  ns and  $\tau_F(2p_{1/2})=1.73$  ns), and for all other ion energies,  $F=600$  V/cm (in this case  $\tau_F(2s)=5.04$  ns and  $\tau_F(2p_{1/2})=2.33$  ns). It was necessary to decrease the field strength to 150 V/cm for  $E=1.15$  MeV to keep the charged particles deflected from the  $z$  axis in the quenching field from being deflected outside the aperture of the guard electrode (Fig. 1) of the Faraday cylinder.

Electrons and ions formed in the target gas under the action of the impinging particles are accelerated by the field of the quenching capacitor and, bombarding the surface of its plates, are capable of generating radiation in the range of spectral sensitivity of the photomultiplier. Experimental confirmation in a proton beam with varying energy  $E$  at high target densities, when  $\sigma_i t \geq 1$ , where  $\sigma_i$  is the ionization cross section of the gas,<sup>22</sup> comparing the cases of fields in the range  $F=500-800$  V/cm with no field, has shown that the contribution of this and similar processes to the total number  $N_r$  of recorded photons is negligibly small.

In the course of the measurements of  $\sigma_{i0}(p)$  the plates of the quenching capacitor were shorted out with each other and the housing of the ion pipe to eliminate induced and residual electric fields. However, any particle moving with velocity  $\mathbf{v}$  in a magnetic field with induction  $\mathbf{B}$  is acted upon by the so-called induction field,<sup>21</sup> whose intensity, obviously, is given by the vector product  $\mathbf{F}=[\mathbf{v}\mathbf{B}]$ . Therefore for the hydrogen atom energies obtaining in our experiment even moderate magnetic fields (not more than 5–7 times the Earth's field) create significant induced electric fields, efficiently quenching the metastable state of the hydrogen atoms (Fig. 4) and introducing an uncontrollable error in the photon number  $N_r(2p)$ . In order to eliminate this effect, the collision chamber was protected by a multilayer magnetostatic screen.

As we will see below [see formula (12)], to determine the cross section  $\sigma_{i0}(2s;2p)$  it is necessary to establish a correspondence between the number of recorded  $L_\alpha$  photons and the number  $N_1(0)$  of  $H^-$  ions that have entered the collision chamber. The quantity  $N_1(0)$  is measured with the help of the Faraday cylinder (Fig. 1). As a result of the interaction of the  $H^-$  ions and the gas in the collision chamber, the particle beam propagating along the ion pipe, in the region of the Faraday cylinder, consists of a mixture of fast  $H^-$ ,  $H^+$ , and  $H^0$  particles, and also electrons and slow ions, i.e., target fragments. To measure  $N_1(0)$  it is necessary to separate out from such a beam only the flux of high-energy hydrogen particles. Toward this end, a sheet of aluminum foil of thickness 4 mm was placed in the path, this thickness being much less than the mean free path of protons with energies greater than 1 MeV in aluminum, to hold back the flux of slow ions and electrons and convert any hydrogen particles into protons. Behind the aluminum foil the proton beam, whose number is equal to  $N_1(0)$ , is accompanied by a flux of for the most part low-energy convoy electrons.

To eliminate errors in determining  $N_1(0)$  associated with the presence of the convoy electrons and the reverse flux of secondary electrons emitted by the Faraday cylinder, a guard

electrode was placed between the aluminum foil and the Faraday cylinder, with diameter of the opening for the beam equal to 6 mm and to which was applied a negative voltage  $U$  with respect to the grounded foil and Faraday cylinder (through an ammeter). To lower the potential on the ground electrode the current from the Faraday cylinder due to the proton beam was varied from its starting value at  $U=0$  to some limiting value, which was reached for  $U=-300-400$  V and from there on remains practically constant. All remaining measurements were made at  $U=-450$  V. The current (charge) delivered by the protons to the Faraday cage was measured by an integrating current-frequency converter (the same as a charge-pulse number converter) with an error of  $\pm 10\%$ . The total leakage currents of the measuring channel did not exceed  $5 \cdot 10^{-4}$  A, which is two orders of magnitude lower than the  $H^-$  ion current.

### 3. CALCULATION OF THE $\sigma_{i0}(2s)$ and $\sigma_{i0}(2p)$ CROSS SECTIONS FROM THE EXPERIMENTAL DATA

In general, the equation for the particle distribution in the beam as a function of the species of which it is composed and their electronic states, both in the gaseous target and outside it, should contain a term reflecting collision processes with and without change of the charge of the particles, a term taking into account changes in the populations of the electronic states of the particles due to spontaneous transitions, and a term that describes the various auto-ionization processes:

$$d\Phi_i^{(\nu)}(z) = n(z) \sum_j \sum_\mu [\Phi_j^{(\mu)} \sigma_{ji}(\mu - \nu) - \Phi_i^{(\nu)} \sigma_{ij}(\nu - \mu)] dz + \sum_\mu [\Phi_i^{(\mu)} dP_i(\mu - \nu) - \Phi_i^{(\nu)} dP_i(\nu - \mu)] + \sum_\mu \sum_\gamma [\Phi_{i-1}^{(\mu)} dP_{i-1,i}(\mu - \nu) - \Phi_i^{(\nu)} dP_{i,i+1}(\nu - \gamma)] + \dots, \quad (9)$$

where  $\Phi_i^{(\nu)}(z)$  is the fraction of particles in the beam with charge  $i$  and electronic state  $\nu$  as a function of the spatial coordinate  $z$ ;  $n(z)$  is the target density as a function of  $z$ ;  $\sigma_{ij}(\nu - \mu)$  is the cross section of the collision process in which the charge of the particle changes from  $i$  to  $j$ , and the electronic state, from  $\nu$  to  $\mu$ ;  $dP_i(\nu - \mu) = dz/v \tau(\nu - \mu)$  is the probability of spontaneous transition of a particle with charge  $i$  from the state  $\nu$  to the state  $\mu$  with lifetime  $\tau(\nu - \mu)$  within the length segment  $dz$  for particle speed  $v$ ; and  $dP_{i,i+1}(\nu - \mu)$  is the probability of the auto-ionization process along the segment  $dz$  in which the particle charge is increased by one and the electronic state changes from  $\nu$  to  $\mu$ . In Eq. (9) it is possible to take into account also more complicated auto-ionization processes, and also other forms of interaction (e.g., excitation or ionization of the beam particles by protons).

It is clear that  $\mu = \nu$  in Eq. (9) only when  $j = i$  and  $dP_i(\nu - \mu) \equiv 0$  if  $\mu$  is a higher-energy state than  $\nu$ , and summing over such  $\mu$  turns out to be only a formality. From here

on in the denotation of the ground state of the electronic structure of the particles we will drop the symbol  $\nu$  where it does not lead to misunderstanding. Expression (9) is of a general nature and in individual cases reduces to the relations proposed in Refs. 23–25.

System of equations (9) turns out to be infinite since the number of possible terms is infinite even for the simplest atom, hydrogen. But it substantially simplifies if we take account only of the dominant processes. Since the formation of  $H^-$  ions in auto-ionization states can be completely neglected, the third term in Eq. (9) falls out of consideration. Then, in calculating the cross sections of processes (1), we eliminate in the first approximation those terms in Eq. (9) that reflect the role of cascade transitions from states with  $n \geq 3$ , and also those that reflect the role of excitation processes  $H(1s) + M \rightarrow H(2s; 2p) + M(\Sigma)$  and all other similar interactions  $H(nl) + M \rightarrow H(n'l') + M(\Sigma)$ , which is valid for small target thicknesses. Then, solving Eqs. (9) for the fraction of  $H(2p)$  atoms formed in the beam in process (1) in a target with constant density  $n(z) = \text{const}$  in the absence of a field, we find

$$\Phi_0^{(2p)}(z) = \frac{nv\tau(2p)\sigma_{i0}(2p)}{1 - nv\tau(2p)[\sigma_\Sigma - \sigma_{01}(2p)]} \times \left\{ \exp(-\sigma_\Sigma nz) - \exp\left[-\left[\sigma_{01}(2p)n + \frac{1}{v\tau(2p)}\right]z\right] \right\}, \quad (10)$$

where  $\sigma_\Sigma = \sigma_{i0} + \sigma_{i1}$ .

Generally, the  $\sigma_{01}(2p)$  electron loss cross sections from an excited  $2p$  state of the hydrogen atom are unknown, and therefore experiments are typically carried out at small enough values of the density  $n$  that the inequality  $nv\tau(2p)\sigma_\Sigma \ll 1$  will be fulfilled (note that  $\sigma_\Sigma \approx \sigma_{01}(2p)$ ) and the corresponding expressions in Eq. (10) containing  $\sigma_\Sigma$  and  $\sigma_{01}(2p)$  can be dropped.

Since the spontaneous transition of some arbitrary particle from an excited state  $\nu$  to the state  $\mu$ , accompanied by the appearance of a photon with energy  $h\nu = E_\nu - E_\mu$  takes place according to an exponential law and is characterized by a lifetime  $\tau(\nu - \mu)$ , it is easy to show that the linear flux density of the corresponding photons emitted by given particles moving in the beam with one and the same velocity  $v$  is given by the expression

$$\frac{dN_{h\nu}(z)}{dz} = \frac{N}{v\tau(\nu - \mu)} \Phi_0^{(\nu)}(z), \quad (11)$$

where  $N$  is the total flux of particles in the beam (with different charges  $i$  and in different states  $\nu$ ). The quantities  $N_i$  and  $dN_{h\nu}/dz$  are functions of time, varying in synchrony with the total flux  $N$  of the particles of the beam. Integrating Eqs. (8) and (11) over the time during which the measurements are made and not changing the notation, we can say that if  $N$  particles of the beam interact with the gas target, the detector will record  $N_r$  photons.

Within the framework of the above assumptions the linear flux density of  $L_\alpha$  radiation formed in the decay of the  $2p$  states of the hydrogen atom, which in turn are produced by process (1), is equal to

$$\frac{dN_{L_\alpha}^{(2p)}(z)}{dz} = N_i(0)\sigma_{i0}(2p)nD, \quad (12)$$

where

$$D(z) = \exp(-\sigma_\Sigma nz) - \exp\left[-\frac{z}{v\tau(2p)}\right].$$

Under these assumptions, but allowing for cascade processes (so that requirements of the form  $nv\tau(nl - 2p)\sigma_\Sigma \ll 1$  must be added), it is possible to ascribe the form (12) to the expression for the linear flux density of the Lyman- $\alpha$  photons with this one difference that the cross section  $\sigma_{i0}(2p)$  appearing as a factor in this expression will be replaced by the following sum:

$$\sigma_{L_\alpha}(2p) = \sigma_{i0}(2p) + \alpha\sigma_{i0}(3s) + \beta\sigma_{i0}(3d) + \dots, \quad (13)$$

where  $\alpha, \beta$ , etc., are weighting coefficients which reflect the contribution to the  $L_\alpha$  intensity due to cascade processes to the  $2p$  level, respectively, from the  $3s, 3d$  states, etc. The analytic form of the coefficients  $\alpha$  and  $\beta$  is determined by which cascade processes are included in the calculation when solving system of equations (9). The cross sections  $\sigma_{i0}(nl)$  decay rapidly with growth of the principal quantum number  $n$  (for  $n \geq 3$ , roughly as  $n^{-3}$ , Refs. 6, 26), for which reason it is expedient to take into account only transitions from the level  $n=3$ . Thus, the coefficients  $\alpha$  and  $\beta$  are calculated using expressions of the same form:

$$\left(\frac{\alpha}{\beta}\right) = 1 - \frac{\tau(3l - 2p)}{\tau(3l - 2p) - \tau(2p)} \left\{ \exp\left[-\frac{z}{v\tau(3l - 2p)}\right] - \exp\left[-\frac{z}{v\tau(2p)}\right] \right\} D^{-1}, \quad (14)$$

where  $l=s$  for the coefficient  $\alpha$  and  $l=d$  for  $\beta$ , and the condition of applicability of formula (14) is  $nv\tau(3l - 2p)\sigma_\Sigma \ll 1$ .

Such expressions can be obtained for the decay of the  $2s$  states of fast hydrogen atoms that appear as products of reaction (1) in an electric field. In particular, formula (12) is valid if we replace the cross section  $\sigma_{L_\alpha}(2p)$  and lifetime  $\tau(2p)$ , respectively, by  $\sigma_{L_\alpha}(2s)$  and  $\tau_F(2s)$ .

Thus, expressions (8) and (12) allow us to obtain the values of the cross sections  $\sigma_{L_\alpha}(2s; 2p)$  from the measured values  $N_r$  and  $N_i(0)$ , which, as can be seen from Eq. (13), are not exactly the desired cross sections  $\sigma_{i0}(2s; 2p)$  but rather contain some positive added term due to the cascade processes, i.e., the cross sections  $\sigma_{L_\alpha}(2s; 2p)$  give an upper bound on  $\sigma_{i0}(2s; 2p)$ .

If an electric field is turned on (with field strength  $F$ ), the linear flux density of the  $L_\alpha$  radiation at the observation point  $z$  consists of a sum of linear flux densities which char-

acterize the  $L_\alpha$  transitions ( $2p-1s$ ) and ( $2s-1s$ ) in the hydrogen atoms formed in the  $2p$  and  $2s$  states by neutralization (1) of  $H^-$  ions:

$$\frac{dN_{L_\alpha}(z)}{dz} = \frac{dN_{L_\alpha}^{(2p)}}{dz} + \frac{dN_{L_\alpha}^{(2s)}}{dz}. \quad (15)$$

In turn, these terms are determined from the cross sections of formation and interaction with the target and from the lifetimes of the hydrogen atoms in the corresponding excited state both in the interval  $[l]$  between the entrance window of the collision chamber and the quenching capacitor, i.e., outside the field  $F$ , and in the interval  $[z-l]$ , where the electric field is acting (Fig. 1), and are given by expressions of the form

$$\frac{dN_{L_\alpha}^{(2l)}}{dz} = \frac{dN_{L_\alpha}^{(2l)}}{dz} \Big|_{[l]} + \frac{dN_{L_\alpha}^{(2l)}}{dz} \Big|_{[z-l]}, \quad (16)$$

where  $(2l) = (2p)$  or  $(2s)$ . Since under the conditions of our experiment the distance  $l$  and the values of the density  $n$  of the target gas are quite small, in analogy with the derivation of Eqs. (12)–(14) we obtain the following expressions for the linear flux densities entering into Eq. (16):

$$\begin{aligned} \frac{dN_{L_\alpha}^{(2p)}}{dz} \Big|_{[l]} &= N_i(0) \sigma_{L_\alpha}(2p) \frac{n \tau(2p)}{\tau_F(2p)} \exp\left[-\frac{z-l}{v \tau_F(2p)}\right] \\ &\times \left\{ 1 - \exp\left[-\frac{l}{v \tau(2p)}\right] \right\}, \end{aligned} \quad (17)$$

$$\frac{dN_{L_\alpha}^{(2s)}}{dz} \Big|_{[l]} = N_i(0) \sigma_{L_\alpha}(2s) \frac{nl}{v \tau_F(2s)} \exp\left[-\frac{z-l}{v \tau_F(2s)}\right], \quad (18)$$

$$\begin{aligned} \frac{dN_{L_\alpha}^{(2p)}}{dz} \Big|_{[z-l]} &= N_i(0) \exp(-\sigma_\Sigma nl) \sigma_{L_\alpha}(2p) n \\ &\times \left\{ \exp[-\sigma_\Sigma n(z-l)] - \exp\left[-\frac{z-l}{v \tau_F(2p)}\right] \right\}, \end{aligned} \quad (19)$$

$$\begin{aligned} \frac{dN_{L_\alpha}^{(2s)}}{dz} \Big|_{[z-l]} &= N_i(0) \exp(-\sigma_\Sigma nl) \sigma_{L_\alpha}(2s) n \\ &\times \left\{ \exp[-\sigma_\Sigma n(z-l)] - \exp\left[-\frac{z-l}{v \tau_F(2s)}\right] \right\}, \end{aligned} \quad (20)$$

where  $\tau_F(2p)$  is the effective lifetime of the  $2p_{1/2,3/2}$  states of the hydrogen atom in an electric field with field strength  $F$ . It is necessary to bear in mind that the cross sections  $\sigma_{L_\alpha}(2s;2p)$  found from Eqs. (17) and (18) differ somewhat from the same cross sections obtained from Eqs. (19) and (20) since the contribution to  $\sigma_{L_\alpha}(2s;2p)$  from the cascade processes is different in an electric field.

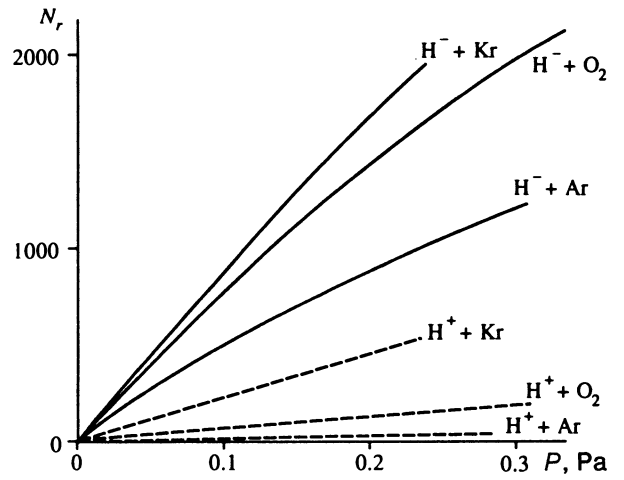


FIG. 5. Dependence of the number of recorded photons  $N_r$  on the pressure  $P$  of target gases Ar, Kr, and  $O_2$  bombarded by  $H^+$  and  $H^-$  ions with energy  $E = 1.15$  MeV.

The method for calculating the cross sections  $\sigma_{L_\alpha}(2s)$  consists in the following. The quantity  $\sigma_{L_\alpha}(2p)$ , calculated with the help of formulas (8) and (12) from the measurements in the absence of a field, together with other experimental parameters, is substituted in expressions (17) and (19), and the latter are then substituted into relation (16) in order to find the flux density  $dN_{L_\alpha}^{(2p)}/dz$ . Due to the discovered value of this density, Equation (15), and the observed in the electric field value,  $dN_{L_\alpha}/dz$ , we will find the value  $dN_{L_\alpha}^{2s}/dz$ . Turning now to expressions (18) and (20) and the sum (16) written for the function  $dN_{L_\alpha}^{(2s)}/dz$ , we determine the cross section  $\sigma_{L_\alpha}(2s)$ .

Note that for  $E = 10.4$  MeV the increase in the cross sections  $\sigma_{L_\alpha}(2s)$  associated with taking account of the change in the lifetimes of the  $2p_{1/2,3/2}$  states in an electric field does not exceed 2%. At lower collision energies such an increase is still smaller and can be completely neglected, i.e., we can set  $\tau_F(2p) = \tau(2p)$ .

#### 4. MEASUREMENT RESULTS

In the measurement of the cross sections  $\sigma_{L_\alpha}(2s;2p)$  it was important to make sure that the radiation recorded by the photomultiplier was due to the interaction of the  $H^-$  ions with the gas target and not to any secondary processes (such as  $H^0 + M$ ;  $H^+ + M$ ;  $e^- + M$ , etc.). Toward this end, we carefully examined the dependence of the intensity of the detected radiation on the gas pressure in the collision chamber. We found out that secondary processes can make a substantial contribution to the number of recorded photons at large values of the gas density  $n$  (equivalently, pressure  $P$ ). As a result, the function  $N_r(P)$  remains linear where, according to Eqs. (8) and (12), it should show a noticeable change in slope (see Fig. 5), and the calculated cross sections  $\sigma_{L_\alpha}(2p)$  grow systematically with increase of the gas density  $n$ . This circumstance was taken into account in the calculation of  $\sigma_{L_\alpha}(2p)$  and  $\sigma_{L_\alpha}(2s)$ : the calculations were car-

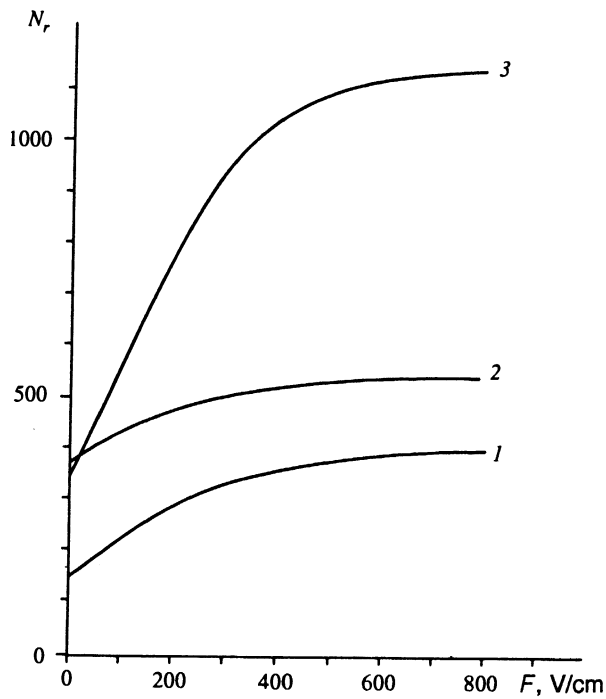


FIG. 6. Dependence of the number of recorded photons  $N_r$  on the electric field strength  $F$  created by the quenching capacitor for  $H^-$  ions with energy  $E=10.4$  MeV and the following target gases: 1) He (for density  $n=4.65 \cdot 10^{14}$  cm $^{-3}$ ), 2)  $H_2$  ( $n=6.63 \cdot 10^{13}$  cm $^{-3}$ ), 3) Ar ( $n=9.44 \cdot 10^{13}$  cm $^{-3}$ ).

ried out for gas densities such that at the moment the beam passed through the region from which the  $L_\alpha$  radiation originated it was possible to interact 10–15% of the primary  $H^-$  ions with the target, i.e., under conditions under which the role of secondary processes was insignificant.

The influence that the radiation of the atoms or molecules of the target have on the magnitude of the  $\sigma_{\bar{1}0}(2s;2p)$  cross sections can be estimated by recording the radiation excited in the gas by a beam of protons of the same intensity and energy as those of the  $H^-$  ion beam. Since protons with energies  $E \geq 1$  MeV possess relatively small electron-capture cross sections,<sup>1,27</sup> all of the emerging radiation is the result of de-excitation of the target particles. Such measurements of  $N_r(M)$ , the number of recorded photons generated by the target gas, were carried out for the proton energies  $E=1.15, 5.0,$  and  $10.4$  MeV. At the same gas pres-

TABLE I. Cross sections of hydrogen atom production in the  $2p$  and  $2s$  states by neutralization of  $H^-$  ions with energy  $E=1.15$  MeV in various gas targets ( $\alpha=0.147, \beta=0.804$ ). The cross sections are given in units of  $10^{-18}$  cm $^2$ , the gas density in units of  $10^{13}$  cm $^{-3}$ .

Gas	$n$	$N_r(M)$	$N_r(2p)$	$N_r(2s;2p)$	$\sigma_{L_\alpha}(2p)$	$\sigma_{L_\alpha}(2s)$
He	14.9	29.7	458	1003	2.72	4.36
Ar	1.11	5.70	272	433	21.0	44.8
Kr	5.58	550	1848	2730	23.8	53.4
Xe	1.29	237	760	...	42.4	...
$H_2$	4.45	609	2256	2690	36.4	10.3
$O_2$	5.54	128	1622	2903	21.0	44.0
$CO_2$	1.91	...	990	1951	37.2	77.4

TABLE II. Cross sections of hydrogen atom production in the  $2p$  and  $2s$  states by neutralization of  $H^-$  ions with energy  $E=5.0$  MeV in various gas targets ( $\alpha=0.069, \beta=0.516$ ). The cross sections are given in units of  $10^{-18}$  cm $^2$ , the gas density in units of  $10^{13}$  cm $^{-3}$ .

Gas	$n$	$N_r(M)$	$N_r(2p)$	$N_r(2s;2p)$	$\sigma_{L_\alpha}(2p)$	$\sigma_{L_\alpha}(2s)$
He	16.6	8.50	143	500	0.666	1.72
Ar	2.45	5.03	248	914	8.26	22.8
Kr	1.86	72.9	352	1040	13.6	31.0
Xe	1.25	111	407	1045	23.4	42.4
$H_2$	2.23	174	300	467	9.80	5.62
$O_2$	3.33	25.8	294	849	6.34	14.3
$CO_2$	2.30	27.3	315	935	9.84	22.8

sure He and Ar atoms and  $O_2$  and  $CO_2$  molecules are excited the most weakly; the intensity of the radiation increases from there on in the order Kr,  $H_2$ , Xe (Fig. 5 and Tables I–IV). For the last three gases the intensity of the radiation induced by the  $H^-$  ions exceeds the corresponding intensity in the case of a proton beam by a factor of only 3–5. For He, Ar,  $O_2$  and  $CO_2$  these intensities differ by a factor of 10–50; the greatest difference is observed for Ar.

However, the main part of the radiation recorded during the collisions of  $H^-$  ions with Kr and Xe targets consists most likely to  $L_\alpha$  photons. In Ref. 28 it was shown that with increase of the atomic number of the target the fraction of collisions in which neutralization of  $H^-$  ions takes place with simultaneous excitation of the target atoms decrease without deviation and, for example, in the case of Xe is determined by a cross section making up  $\approx 8\%$  of the total cross section  $\sigma_{\bar{1}0}$ .

Thus, the cross sections  $\sigma_{L_\alpha}(2s;2p)$  turn out somewhat overestimate the cross sections  $\sigma_{\bar{1}0}(2s;2p)$  not only because of cascade processes, but also as a consequence of target radiation in the spectral sensitivity range of the photomultiplier.

Figure 6 illustrates the dependence of the number of recorded photons on the electric field strength. In fields with  $F \geq 500$  V/cm the linear flux density of the radiation  $dN_{L_\alpha}(z)/dz$  [or, what is the same thing,  $N_r(F)$  for given  $N_{\bar{1}}(0)$ ], reaches saturation as a function of  $F$  since with further increase of  $F$  the lifetime  $\tau_F(2s)$  of the hydrogen atoms does not vary so significantly (Fig. 4) and the exponential  $\exp[-(z-l)/v\tau_F(2s)]$  in expressions (18) and (20) becomes small in comparison with  $\exp[-\sigma_\Sigma n(z-l)]$ , and

TABLE III. Cross sections of hydrogen atom production in the  $2p$  and  $2s$  states by neutralization of  $H^-$  ions with energy  $E=6.9$  MeV in various gas targets ( $\alpha=0.057, \beta=0.452$ ). The cross sections are given in units of  $10^{-18}$  cm $^2$ , the gas density in units of  $10^{13}$  cm $^{-3}$ .

Gas	$n$	$N_r(M)$	$N_r(2p)$	$N_r(2s;2p)$	$\sigma_{L_\alpha}(2p)$	$\sigma_{L_\alpha}(2s)$
He	54.5	...	234	675	0.368	0.744
Ar	8.05	...	388	1152	4.94	10.4
Kr	3.96	...	488	1266	8.86	19.3
Xe	4.74	...	1032	2119	15.7	27.2
$H_2$	2.27	...	170	307	5.44	4.70
$O_2$	15.3	...	707	1756	3.32	8.98
$CO_2$	12.3	...	752	1731	4.40	10.5

TABLE IV. Cross sections of hydrogen atom production in the  $2p$  and  $2s$  states by neutralization of  $H^-$  ions with energy  $E=10.4$  MeV in various gas targets ( $\alpha=0.045$ ,  $\beta=0.376$ ). The cross sections are given in units of  $10^{-18}$   $cm^2$ , the gas density in units of  $10^{13}$   $cm^{-3}$ .

Gas	$n$	$N_r(M)$	$N_r(2p)$	$N_r(2s;2p)$	$\sigma_{L_\alpha}(2p)$	$\sigma_{L_\alpha}(2s)$
He	46.5	9.5	135	394	0.230	0.512
Ar	9.44	...	354	1121	3.70	9.30
Kr	4.29	...	241	770	5.20	12.6
Xe	3.09	93.2	335	782	9.94	15.2
H <sub>2</sub>	6.63	69	352	538	3.92	2.48
O <sub>2</sub>	13.5	37.1	338	1063	2.52	6.20
CO <sub>2</sub>	8.48	21.9	364	900	3.10	6.86

even abrupt changes in it do not have a substantial effect on  $dN_{L_\alpha}/dz$ . Values of the cross sections  $\sigma_{L_\alpha}(2s;2p)$ , calculated according to formulas (8), (12), (15)–(20), are displayed in Tables I–IV. Values of the photon numbers  $N_r(2p)$  for  $F=0$  and  $N_r(2s;2p)$  in a field  $F>0$  for an  $H^-$  ion beam and  $N_r(M)$  for a proton beam for the same target density  $n$  and  $N_1(0) = N_1 = 2.06 \cdot 10^9$  particles are also given in the tables. To give a picture of the influence of cascade processes on the magnitude of the cross sections  $\sigma_{L_\alpha}(2p)$ , the values of the coefficients  $\alpha$  and  $\beta$  calculated according to formula (14) for the case  $n \rightarrow 0$  are given in the explanatory captions to the tables (for the values of  $n$  used in the experiment the condition  $nv\tau(3l-2p)\sigma_\Sigma \ll 1$ , necessary to apply formulas (14), is not as a rule fulfilled). The values of the lifetimes  $\tau(2p)$  and  $\tau(3l-2p)$  used in the calculations were taken from a handbook.<sup>19</sup>

The mean statistical error in the measurement of  $\sigma_{L_\alpha}(2s;2p)$  was  $\pm 35\%$  whereas the absolute values of the  $\sigma_{L_\alpha}(2s;2p)$  cross sections, which are associated with errors in the determination of the absolute value of the sensitivity of the photocathode of the photomultiplier, the effective solid angle of reception, etc., are given with a resultant error of  $\pm 70\%$ .

## 5. CONCLUSION

1. The cross sections  $\sigma_{L_\alpha}(2s;2p)$  for He within the limits of statistical error of the measurements depend on the energy of the  $H^-$  ions according to the law  $E^{-1}$ , which agrees with theoretical results.<sup>3,29</sup> As one goes to heavier atomic gases or molecular gases composed of the atoms of heavier chemical elements, the dependence of  $\sigma_{L_\alpha}(2s;2p)$  on the energy weakens and begins to behave in a manner analogous to the functions  $\sigma_{01}(E)$  and  $\sigma_{10}(E)$  (see Refs. 14, 15, and 27).

2. The absolute values of the cross sections  $\sigma_{L_\alpha}(2s;2p)$  grow with increase of the atomic number of the target. The character of this variation is similar to the dependence of  $\sigma_{10}$  on the type of target.<sup>14,15,27</sup>

3. According to the above two points, the ratios  $\sigma_{L_\alpha}(2s \text{ or } 2p)/\sigma_{10}$ , as functions of the  $H^-$  ion energy, remain approximately constant for all types of targets and equal to  $\sigma_{L_\alpha}(2p)/\sigma_{10}=4-7\%$  and  $\sigma_{L_\alpha}(2s)/\sigma_{10}=9-19\%$ . In the case of a target of molecular hydrogen

these ratios grow abruptly, which, most probably is due to recording additional radiation from the target particles.

4. The  $\sigma_{L_\alpha}(2s)$  cross sections exceed the  $\sigma_{L_\alpha}(2p)$  cross sections by a factor of 2–2.7 for interaction of  $H^-$  ions with energies  $E=1-11$  MeV with any of the investigated targets. In the low-energy region  $E=5-40$  keV the ratio between the cross sections turns over:  $\sigma_{10}(2p) > \sigma_{10}(2s)$  (Ref. 7).

5. A number of difficulties associated with the measurement of the  $\sigma_{10}(2s)$  cross sections inside the collision chamber can be eliminated by placing the quenching capacitor and the apparatus for recording the  $L_\alpha$  radiation outside the collision chamber. Errors in the determination of  $\sigma_{10}(2s)$  due to target radiation and  $L_\alpha$  radiation from  $H(2p)$  atoms then disappear and the possibility arises of taking more accurate account of cascade transitions and polarization of the radiation. However, the intensity of the  $L_\alpha$  radiation of the  $H(2s)$  atoms moving along the  $z$  axis in the field of the capacitor will be a periodically varying function of  $z$  (the effect of “quantum beats,” Refs. 15, 30), which must be taken into consideration in the development of the measuring technique.

The authors express their deep gratitude to A. L. Shalyapin and A. A. Lukichev for carrying out a number of tasks in the construction of the optical channel and for determining the quantum efficiency of recording of the Lyman- $\alpha$  radiation of the hydrogen atoms, and also to B. V. Shul'gin for his interest and support of this work.

For the formulation of the problem we are indebted to R. A. Demirkhanov and D. V. Chkuaseli.

<sup>1</sup>H. S. W. Massey, *Negative Ions* [Russian translation], Nauka, Moscow (1979).

<sup>2</sup>L. D. Landau and E. M. Lifshitz, *Quantum Mechanics*, Pergamon Press, Oxford (1974).

<sup>3</sup>E. P. Dewangan and H. R. J. Walters, *J. Phys. B* **11**, 3983 (1978).

<sup>4</sup>V. Dose and U. Schmocker, *Z. Phys. A* **275**, 325 (1975).

<sup>5</sup>J. Geddes, J. Hill, and H. B. Gilbody, *J. Phys. B* **14**, 4837 (1981).

<sup>6</sup>M. Harnois, R. A. Falk, R. Geballe, and J. Risley, *Phys. Rev. A* **16**, 2256 (1977).

<sup>7</sup>A. L. Orbeli, E. P. Andreev, V. A. Ankudinov, and V. M. Dukel'skiĭ, *Zh. Ėksp. Teor. Fiz.* **58**, 1938 (1970) [*Sov. Phys. JETP* **31**, 1044 (1970)].

<sup>8</sup>D. W. Sida, *Proc. Phys. Soc. A* **68**, 240 (1955).

<sup>9</sup>M. R. C. McDowell and G. Peach, *Proc. Phys. Soc.* **74**, 463 (1959).

<sup>10</sup>M. H. Day, *Phys. Rev. A* **26**, 1260 (1982).

<sup>11</sup>C.-R. Liu and A. F. Starace, *Phys. Rev. A* **40**, 4926 (1989).

<sup>12</sup>C.-R. Liu and A. F. Starace, *Phys. Rev. A* **42**, 2684 (1990).

<sup>13</sup>V. I. Radchenko, *Zh. Ėksp. Teor. Fiz.* **103**, 40 (1993) [*JETP* **76**, 22 (1993)].

<sup>14</sup>V. I. Radchenko, *Zh. Ėksp. Teor. Fiz.* **105**, 834 (1994) [*JETP* **78**, 445 (1994)].

<sup>15</sup>V. I. Radchenko, G. D. Ved'manov, *Zh. Ėksp. Teor. Fiz.* **107**, 3 (1995) [*JETP* **80**, 1 (1995)]. (1994)].

<sup>16</sup>E. P. Andreev, V. A. Ankudinov, and S. V. Bobashev, *Zh. Ėksp. Teor. Fiz.* **50**, 565 (1966) [*Sov. Phys. JETP* **23**, 375 (1966)].

<sup>17</sup>I. C. Percival and M. J. Seaton, *Phil. Trans. R. Soc. A* **251**, 113 (1958).

<sup>18</sup>W. Pauli, *Theory of Relativity*, Dover, New York (1983).

<sup>19</sup>A. A. Radtsig and B. M. Smirnov, *Parameters of Atoms and Atomic Ions: Handbook* [in Russian], Energoatomizdat, Moscow (1986).

<sup>20</sup>H. A. Bethe and E. E. Salpeter, *Quantum Mechanics of One- and Two-Electron Systems*, Springer-Verlag, Berlin (1960).

<sup>21</sup>W. E. Lamb and R. C. Rutherford, *Phys. Rev.* **79**, 549 (1950).

<sup>22</sup>J. B. Hasted, *Physics of Atomic Collisions*, Butterworths, London (1965).

<sup>23</sup>K. H. Berkner, S. N. Kaplan, G. A. Paulikas, and R. V. Pyle, *Phys. Rev.* **138**, 410 (1965).

<sup>24</sup>H. Homma, R. R. Lewis, and R. T. Robiscoe, *Phys. Rev. A* **25**, 333 (1982).

<sup>25</sup>V. A. Ankudinov, S. V. Bobashev, and E. P. Andreev, *Zh. Ėksp. Teor. Fiz.* **48**, 40 (1965) [*Sov. Phys. JETP* **21**, 26 (1965)].

- <sup>26</sup>J. C. Rislely, F. J. De Heer, and C. B. Kerkdijk, *J. Phys. B* **11**, 1783 (1978).  
<sup>27</sup>N. V. Fedorenko, *Zh. Tekh. Fiz.* **40**, 2481 (1970) [*Sov. Phys. Tech. Phys.* **15**, 1947 (1970)].  
<sup>28</sup>G. H. Gillespie, *Phys. Rev. A* **16**, 943 (1977).  
<sup>29</sup>G. F. Drukarev, *Zh. Éksp. Teor. Fiz.* **58**, 2210 (1970) [*Sov. Phys. JETP* **31**, 1193 (1970)].

- <sup>30</sup>E. B. Aleksandrov, *Usp. Fiz. Nauk* **107**, 595 (1972) [*Sov. Phys. Usp.* **15**, 436 (1972)].  
<sup>31</sup>E. B. Aleksandrov, N. I. Kaliteevskii, and M. P. Chaika, *Usp. Fiz. Nauk* **129**, 155 (1979) [*Sov. Phys. Usp.* **22**, 760 (1979)].

Translated by Paul F. Schippnick